# Microstructural Investigation of Discarded NdFeB Magnets after Low-Temperature Hydrogenation

Alireza Habibzadeh*[1], Mehmet Ali Kucuker[2], Öznur Çakır[3,4], Mertol Gökelma[1]

[1] Department of Materials Science and Engineering, İzmir Institute of Technology, Izmir, 35433, Turkey

[2] Department of Environmental Engineering, İzmir Institute of Technology, Izmir, 35433, Turkey

[3] Turkish Energy and Mineral Research Agency / Rare Earth Elements Research Institute,Ankara,06980,Turkey

[4] Department of Metallurgical and Materials Engineering, Yildiz Technical University, Istanbul, 34220, Turkey,

*Corresponding Author's E-mail and Phone: alirezahabibzadeh@iyte.edu.tr, +905515972042

## Abstract

With the imposition of some restrictions on the export of rare earth elements (REEs) by China, a dominant producer of these elements, the supply of REEs will soon be a challenge. To mitigate the supply risk of REEs, a lot of attention has been paid to recycling recently. Despite the more common recycling methods, including hydrometallurgical and pyrometallurgical processes, the hydrogen processing of magnetic scrap (HPMS) is still in the development stage. Magnet-to-magnet recycling via hydrogenation of end-of-life (EoL)NdFeB magnets provides a fine powder suitable for the production of new magnets from secondary sources. One of the crucial aspects of HPMS is the degree of recovery of the magnetic properties, as the yield efficiency can easily reach over 95%. The amount, morphology, and distribution of the Nd-rich phase are the key parameters to achieve the highest maximum energy product $(BH)_{max}$ by isolating the matrix grain. Therefore, a better insight into the microstructure of the matrix grains and the Nd-rich phase before and after hydrogenation is an important aspect in terms of restoring the final magnetic properties. In this study, a low-temperature hydrogenation process in the range of room temperature to 400 °C was conducted to recycle NdFeB magnets from discarded hard disk drives (HDDs), and the hydrogenated powder was characterized by electron microscopy and X-ray diffraction. The results show that there are three different morphologies of the Nd-rich phase, which undergo two different transformations through oxidation and hydride formation. While at lower temperatures (below 250 °C) the degree of pulverization is higher and the experimental evidence of hydride formation is less clear, the opposite is true at higher temperatures. The formation of neodymium hydride at higher temperatures prevents further oxidation of the Nd-rich phase due to its high stability.

**Keywords:** Hydrogen decrepitation, Magnet-to-magnet recycling, Nd-rich phase, HPMS

# 1. Introduction

The sintered neodymium-iron-boron (NdFeB) permanent magnets introduced in the 1980s are used in a variety of applications due to their excellent magnetic properties [1]. The permanent magnet industry, which relies mainly on NdFeB rather than samarium-cobalt (Sm-Co) magnets due to the high price and rarity of Sm and the avoidance of the use of strategic Co metal, consumes around 23% of all REEs produced worldwide [2, 3]. China's dominance in the REE market and recently imposed export restrictions, combined with the ever-increasing demand for REEs, have resulted in these materials being at the top of the European Commission's list of Critical Raw Materials (CRMs) [4, 5]. Therefore, recycling of discarded NdFeB permanent magnets, containing Nd, Pr, Dy, Gd, and Tb, has recently received huge attention to alleviate the supply risk, however, it is still in the development stage and there is no established industrial procedure [6].

Common methods for the recovery of REEs from discarded NdFeB magnets include pyrometallurgical routes such as electroslag refining, liquid metal extraction, and direct remelting or hydrometallurgical routes such as direct leaching in mineral acids, leaching with oxidative roasting, leaching with chlorination roasting and bioleaching [4, 7, 8]. All of these recycling processes focus on the recovery of elemental rare earth through the production of rare earth oxides and the subsequent energy-intensive molten salt electrolysis step. However, hydrogen processing of magnetic scrap (HPMS) focuses on magnet-to-magnet recycling and skips some energy-intensive steps which also have a high environmental impact [9].

HPMS, as one of the most promising methods for magnet-to-magnet recycling with an efficiency of over 90% [10], has recently attracted much attention and has been carried out by low- and high-temperature hydrogenation [9]. It is believed that low-temperature hydrogenation, also called hydrogen decrepitation (HD), relies only on the formation of $NdH_x$ from the Nd-rich grain boundary phase and pulverization due to the local expansion between the matrix grains, resulting in the collapse of the whole structure of the magnet [11]. The obtained powder can be directly used for further processing, including pressing, aligning, vacuum sintering, coating, and magnetization to manufacture new sintered magnets [12].

The mechanism of hydrogen decrepitation at the microstructural level is based on the high diffusivity of hydrogen atoms, which penetrate into the Nd-rich grain boundary phase and the interstitial sites of the $Nd_2Fe_{14}B$ matrix grains (φ-phase) and lead to the formation of $NdH_x$ and $Nd_2Fe_{14}BH_x$ [3, 13]. Moreover, on the one hand, the formation of $Nd_2Fe_{14}BH_x$ with higher hydrogen content (higher value of x) decreases the magnetocrystalline anisotropy and the preferred magnetization direction of the magnet by weakening the magnetic interaction between the magnetic elements (Nd and Fe) [14]. On the other hand, the formation of $NdH_x$ can protect the Nd-rich phase from oxidation due to its high stability, which is crucial for the recovery of magnetic properties in the final stage of magnet-to-magnet recycling [15]. Since the final magnetic properties of recycled NdFeB magnets are highly dependent on the microstructure and distribution of the Nd-rich phase, a microstructural study of the hydrogenated powder is required [16].

The high maximum energy product $(BH)_{max}$ of NdFeB magnets is attributed to its microstructure, in which the tetragonal $Nd_2Fe_{14}B$ grains (φ-phase) are surrounded and isolated by the Nd-rich grain boundary phase (intergranular) [17, 18]. In addition to the φ-phase and the Nd-rich grain boundary phase, the presence of a B-rich phase with a very low content has also been reported by various researchers [1, 19, 20]. The Nd-rich phase, which is the result of the addition of extra Nd in the manufacturing process, causes the formation of a thin continuous layer surrounding the matrix grains and prevents the nucleation of the reverse magnetic domain by the formation of core-shell structures [9, 21]. Therefore, the degree of wetting and penetration of the Nd-rich grain boundary phase between the matrix grains, which is the key factor in achieving the highest performance of the magnet, can be significantly and differently influenced by the initial chemical composition [22]. First, the Nd content in the magnet can strongly influence the presence of Nd in the Nd-rich phase. Koyama et al [23] reported that when the initial Nd content in the magnet is reduced from 15% to 12%, the Nd content in the Nd-rich grain boundary phase decreases from 80% to 30%. Secondly, the presence of some alloying elements such as Al and Cu can reduce the wetting angle facilitate penetration, and promote complete coverage of the matrix grain in the presence of a liquid Nd-rich phase [24, 25]. Thirdly, additional

alloying elements such as Dy and Tb, which are generally added to the magnet in the form of hydride ($DyH_3$ and $TbH_2$), form a single or double layer of core-shell structure and improve the magnetic isolation of the matrix grain, leading to an increase in the coercivity of the produced magnet [26, 27].

Due to its complexity, various experimental research has been conducted to identify the crystal structure, chemical composition, and morphology of the Nd-rich grain boundary phase to have a better understanding in the last decades. The Nd-rich grain boundary phase is composed of mostly Nd (always accompanied by Pr), some Fe, O, and maybe some traces of B [20, 28, 29]. As a result, the different microstructure and crystal structure of the Nd-rich grain boundary phase have been reported including amorph, cubic, and hexagonal [25, 30, 31]. The amorph Nd-rich grain boundary phase was observed when the boundary thickness is less than 3 μm and changes to crystalline form by increasing the boundary thickness [32]. It is reported by Shinba et al. [33], that a post-sinter annealing treatment causes the formation of a smooth and amorph Nd-rich phase which can cover the mtrix grains more efficiently (high wettability). In addition, Mo et al. [20] reported that the complexity of the crystal structure of the Nd-rich phase is due to the oxygen content, and when oxygen content is increased the crystal structure of the Nd-rich phase changes from double close-packed hexagonal (DHCP) to face-centered cubic (FCC) and finally to close-packed hexagonal (HCP). The morphology, crystal structures, lattice parameters, and oxygen content of the Nd-rich phases were determined by various researchers using transmission electron microscopy (TEM) (see Table 1). The observed diversity in the detected crystal structure may be attributed to the different manufacturing processes and consequently different oxygen absorption rates and could be influenced by the characterization techniques, as it has been reported that the Nd-rich phase may not be completely stable under electron irradiation [34].

**Table 1.** The microstructural characteristics of various Nd-rich grain boundary phases in the literature.

| NO. | Performed Process | Chemical Composition of Magnet | Crystal Structure | Lattice Parameters (nm) | Chemical Composition of Nd-rich Phase (at. %) | Observed Morphology or size | Characteri-zation Techniques | Ref. |
|---|---|---|---|---|---|---|---|---|
| 1 | As sintered 1080°C, 1h | - | DHCP<br>FCC | a: 0.365<br>c: 1.18<br>a: 0.51 | Nd: 90, Fe: 10<br>Nd:70, O:15, Fe: 5 | NA | TEM<br>XRD<br>Auger Spectroscopy | [28] |
| 2 | As cast ingot, Annealed at 1100°C, 1h | $Nd_{15}Fe_{77}B_8$ | FCC<br>Complex BCC<br>Space group $Ia\bar{3}$ | a: 0.52<br>a: 1.04 | Nd - O<br>$Nd_2O_3$ | NA | TEM | [34] |
| 3 | As sintered | $Nd_{15}Fe_{76.5}B_{7.0}Dy_{0.4}Nb_{0.5}Al_{0.6}$ | BCC<br>Space group $Ia\bar{3}$<br>Stable up to 300°C<br>HCP<br>Transformed at 400°C | a: 1.08<br>$La_2O_3$ prototype | $Nd_2O_3$<br>O: 50± 10 %<br>O: 50± 10 % | NA | TEM<br>HREM<br>In situ heating | [35] |
| 4 | As sintered (1050°C) followed by post-annealed (800°C) | $Nd_{15}Fe_{79}B_6$ | Amorph<br>FCC<br>Space group $Ia\bar{3}$ | Thick. < 2<br>a: 0.55<br>a: 1.11 | -<br>-<br>$Nd_2O_3$ | Intergranular phase: sev. hundred nm, Intragrain precipitates: 20-30 to sev. hundred nm | HRTEM<br>EDS | [33] |
| 5 | Sintered, followed by heat treatment (tempered at 600°C, 2h) | $Nd_{22}Fe_{71}B_7$ | DHCP<br>FCC<br>HCP | a: 0.37<br>c: 1.18<br>a: 0.54<br>a: 0.38<br>c: 0.61 | O: < 9, Fe: 7-9<br>Nd: balanced<br>O:11-43, Fe:7-9<br>Nd: balanced<br>O:55-70, Fe:7-9<br>Nd: balanced | NA | TEM<br>XRD<br>EDS | [20] |
| 6 | As sintered<br>Post-sinter annealed | $Nd_{11.7}Pr_{2.8}Fe_{76.8}B_{6.0}Al_{0.5}Cu_{0.1}O_{2.1}$ | DHCP<br>FCC: (Fe, Nd)$O_x$<br>Cubic $NdO_2$<br>Amorphous | a: 0.37<br>c: 1.18<br>a: 0.53<br>a: 0.56<br>Thick.: 3 | O/Nd: 0.05<br>O/Nd: 0.22<br>O/Nd: 2:1<br>$Nd_{30}Fe_{45}Cu_{24.1}B_{0.9}$<br>No Oxygen | NA | HRTEM<br>EDS<br>HRSEM<br>3DAP | [31] |
| 7 | As sintered 1050 °C, 2h | $Nd_{30}(Fe,TM)_{69}B$<br>TM: | FCC | a: 0.55 | - | Different: from hundreds of nm | HRTEM<br>SEM | [30] |

| | | | | | | |
|---|---|---|---|---|---|---|
| Heat treatment:<br>1. 900°C, 2h<br>2. 520°C, 2h | transition metals | BCC | a: 1.1 | - | to several micrometers | EDS |

The reported structure of metallic Nd is DHCP, which is believed to transform into FCC during the sintering process at elevated temperatures (above 1000°C) by absorbing more oxygen, increasing from 0.017 wt% to 0.63 wt% after sintering [20, 28]. Therefore, in some works, the DHCP structure cannot be recognized due to the high oxygen content because the study of the crystal structure was carried out after sintering.

However, an in-depth discussion based on experimental evidence about the microstructural transformation of NdFeB magnets after low-temperature hydrogenation is missing in the literature. Despite the claims made by various researchers [12, 21, 36, 37] about the formation of neodymium hydride after low-temperature hydrogenation and its higher stability based on the ΔG of hydride formation reactions [9], experimental evidence (e.g. XRD characterization) on the detection of NdHx after hydrogenation is not readily accessible or valid. Onel et al. [15] reported that there is no detectable $NdH_x$ after hydrogenation at room temperature. The importance of the formation of neodymium hydride is related to the decreasing reactivity of the obtained powder to prevent oxidation due to the high stability of neodymium hydride at room temperature. Due to the complexity of characterization in the presence of hydrogen and the lack of a clear description of low-temperature hydrogenation or hydrogen decrepitation mechanism in NdFeB magnets in the literature, this work attempts to present a microstructural study of the matrix grain and the Nd-rich grain boundary phase to identify the morphologies, chemical composition, distribution, and all transformations and phenomena after low-temperature hydrogenation in the range of 25 to 400 °C.

## 2. Experimental Procedure

The EoL NdFeB magnets were obtained from discarded IBM hard disk drives (HDDs) manufactured between 2010 and 2014. The HDDs were manually disassembled to extract clean, unoxidized magnets. The extracted NdFeB magnets, weighing approximately 16 g and 4.5 mm thick, were hand-peeled to separate the Ni-Cu coating and prevent nickel from mixing with the final hydrogenated powder.

The NdFeB magnets underwent a multi-step procedure; initially, the raw magnet was broken with a hammer to prepare a cross-section for scanning electron microscopy with energy dispersive spectroscopy (SEM-EDS) and milling to prepare powders for inductively coupled plasma mass spectrometry (ICP-MS) and X-ray diffraction (XRD) to analyze the microstructure and identify phases prior to hydrogenation. Subsequently, the decoated magnet was hydrogenated at different temperatures for two hours.

The experimental setup for hydrogenation depicted in Fig. 1, involved placing the magnet inside a stainless-steel reactor with a volume of about 3 liters. The inner atmosphere of the reactor was evacuated three times with a vacuum pump and then filled with hydrogen to remove as much oxygen as possible. Then reactor was positioned in a heat-resistant furnace to reach targeted temperatures. A digital thermocouple continuously monitored the temperature inside the reactor. After reaching the targeted temperatures (in the range of 25-400 °C), the hydrogen gas was blown into the reactor for 2 hours at a flow rate of 1 l/min while maintaining a pressure of 1 bar. After completion of the hydrogenation process, the reactor was removed from the furnace and cooled in the atmosphere. Argon gas was then purged into the reactor, which accumulated at the bottom of the reactor to prevent further oxidation when the lid of the reactor was removed. The powder was then immediately placed in the glovebox for sampling. The atmosphere in the glovebox contains less than 50 ppm of oxygen and a moisture content of less than 100 ppm. After taking samples in a controlled atmosphere, the rest of the powder was subjected to sieving and particle size analysis to determine the effect of hydrogenation on the particle size. Finally, the collected samples were characterized by X-ray diffraction, and SEM-EDX to identify the different phases in terms of morphology, chemical composition, and oxygen content.

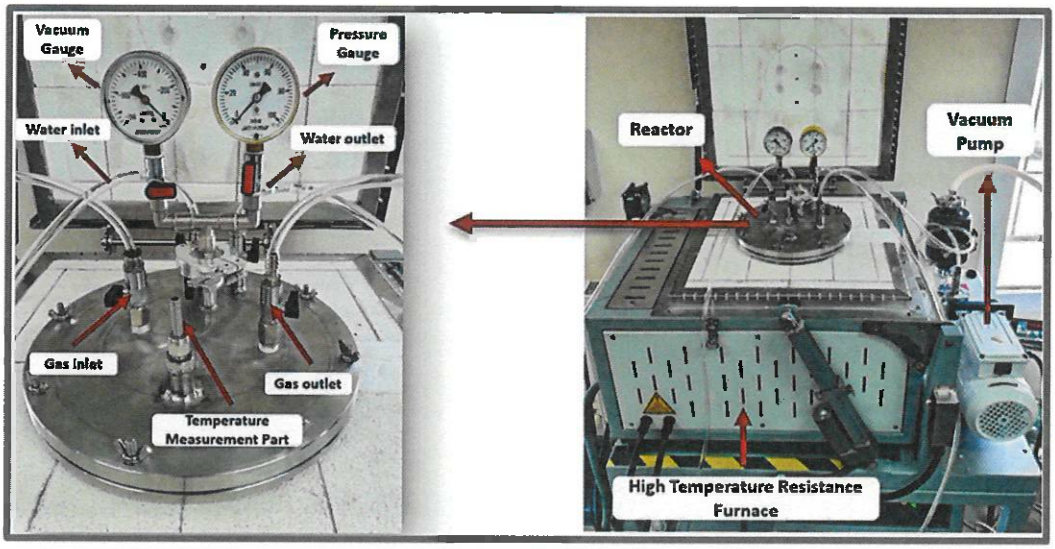



**Fig. 1)** Experimental setup for hydrogenation of EoL NdFeB magnets

## 3. Results and Discussion

The initial chemical composition of the NdFeB magnets which was extracted from the IBM HDDs is tabulated in Table 2. In the following sections, the matrix grain and Nd-rich grain boundary phases were studied before and after hydrogenation.

**Table 2.** The initial chemical composition of the NdFeB magnet extracted from the IBM HDDs

| Element | Fe wt.% | Nd wt.% | Pr wt.% | B wt.% | Co wt.% | Ni wt.% | Cr wt.% | Cu wt.% | Dy wt.% | Gd wt.% |
|---|---|---|---|---|---|---|---|---|---|---|
| weight | 67.5 | 23.33 | 3.87 | 1.01 | 0.75 | 0.31 | 0.11 | 0.11 | 1.08 | 0.885 |

### 3.1. $Nd_2Fe_{14}B$ Matrix Grains

**Before Hydrogenation**

The cross-sectional SEM image of the broken magnet before hydrogenation (Fig. 2) shows that the matrix grains of $Nd_2Fe_{14}B$ ($\varphi$ phase) are found in different grain sizes ranging from 2 to 8 µm in diameter. As reported by Yin et al. [34], the lattice parameter of this tetragonal phase is a = 0.88 nm and c = 1.22 nm and has no lattice defects. Based on the EDS analysis, the matrix grains contain on average about 68 % Fe, 25 % Nd, 6 % Pr, and 1 % B by weight. The chemical composition of the matrix grain thus corresponds to $(Nd,Pr)_{14}Fe_{81}B_5$, and the higher rare earth content compared to $Nd_2Fe_{14}B$ can be attributed to the presence of Pr. It appears that Nd is always accompanied by Pr, with Pr/Nd in the matrix grain being equal to 0.19 to 0.25.

In the X-ray diffraction of the raw magnet shown in Fig. 3, some traces of neodymium oxide can be seen, which is expected due to the high reactivity of Nd and the duration of exposure to air after decoating and milling for sample preparation. In addition, the diffraction pattern doesn't look fully crystalline, which might be due to the milling preparation.

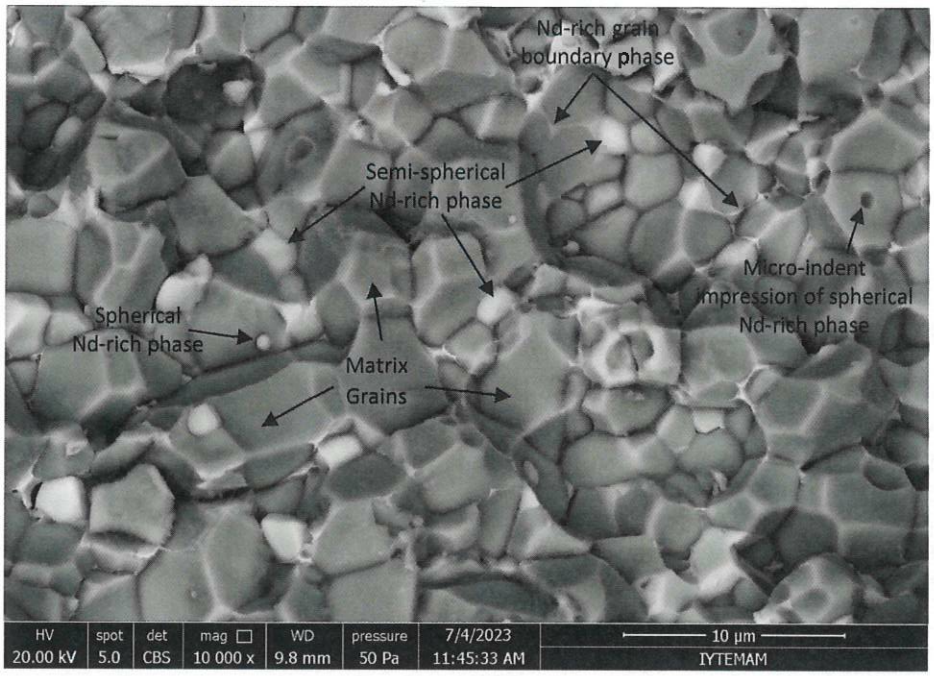



**Fig. 2)** Cross-sectional Backscattered Electron SEM (BSE SEM) image of all phases in the broken raw NdFeB magnet before hydrogenation.

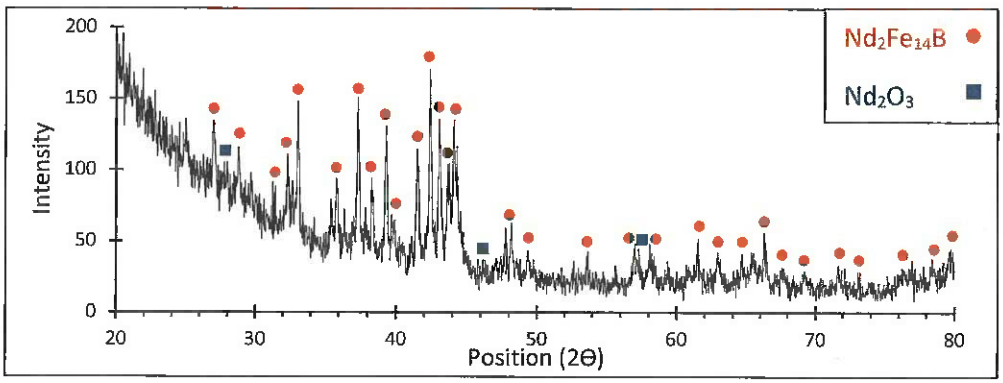



**Fig. 3)** XRD pattern of the broken raw NdFeB magnet before hydrogenation.

**After Hydrogenation**

Fig. 4 shows the X-ray diffraction after low-temperature hydrogenation in the range of 25 – 400 °C, depicting the formation of four different hydrides (different hydrogen content) from the matrix grains and the simultaneous presence of two or three of them at each temperature studied. These results confirm that the hydrogen absorption by the matrix grains varies at different temperatures. In other words, the $Nd_2Fe_{14}B$ is converted to $Nd_2Fe_{14}BH_x$, where x is a function of temperature, but with two opposite trends. First, the value of x in the dominant phase increases from 3.31 to 4.73 when the hydrogenation temperature increases from 25 to 100 °C, and then decreases to 1.04 when the hydrogenation temperature is further increased to 400 °C, showing that hydrogen absorption is highest at 100 °C. This result is also in agreement with Michalsky et al [12]. Isnard et al [13] also reported that the hydrogen atoms have sufficient

diffusivity to penetrate into the interstitial sites of the tetragonal unit cell of the $Nd_2Fe_{14}B$ matrix grain and form a chemical bond with iron atoms.

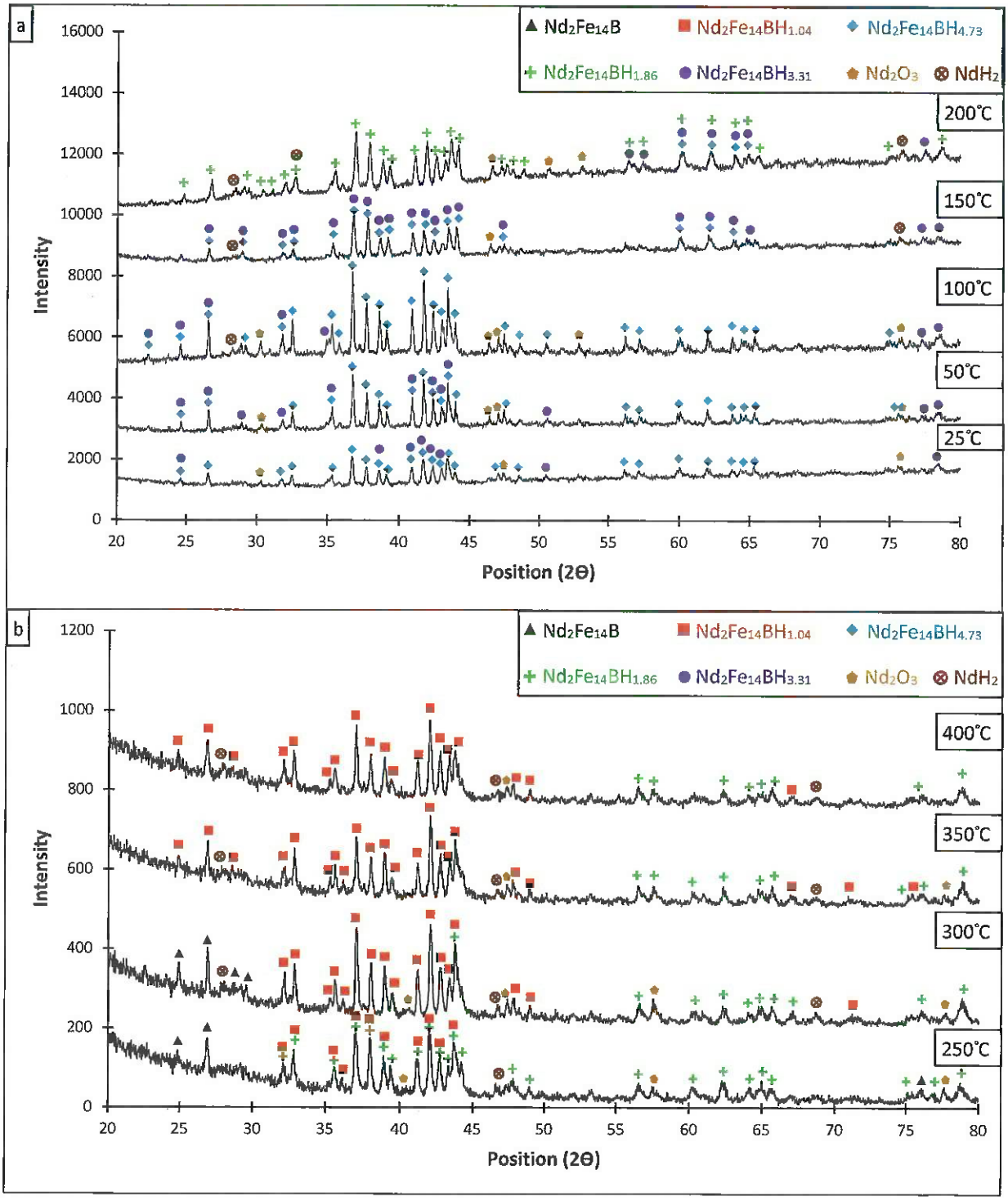



**Fig. 4)** X-ray diffraction pattern of hydrogenated NdFeB magnets at different temperatures; **a)** 25 – 200 °C, and **b)** 250 – 400 °C.

As shown in Fig. 4, each of the four types of $Nd_2Fe_{14}BH_x$ can be identified at different temperatures, but it seems that the hydrogenation temperature of 200 °C is the cut-off point and below that, $Nd_2Fe_{14}BH_{1.04}$ and $Nd_2Fe_{14}BH_{1.86}$ and above that $Nd_2Fe_{14}BH_{3.31}$ and $Nd_2Fe_{14}BH_{4.73}$ cannot be detected, respectively.

Fig. 5 illustrates the mean particle size of the powder obtained after low-temperature hydrogenation in the range of 25 – 400 °C. The particle size analysis shows that the finest particles after hydrogenation can be obtained in the range of 100 to 250 °C, which is almost similar to the trend of X-ray diffraction. In other words, the smallest particle size was obtained at the highest hydrogen uptake. From this one could conclude that the absorption of hydrogen or the formation of $Nd_2Fe_{14}BH_x$ (with different values of x) has a direct effect on the degree of pulverization.

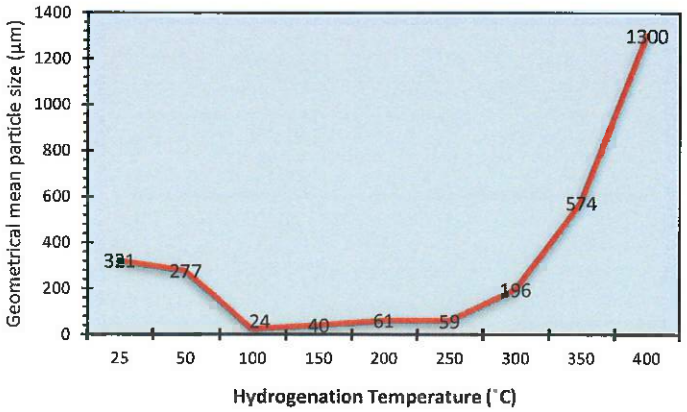



**Fig. 5)** Geometrical mean particle size of the obtained powder after low-temperature hydrogenation of discarded NdFeB magnets.

Other phenomena observed are intergranular cracks in the matrix grain as a result of hydrogenation, as shown in Fig. 6 and also reported by Kilner et al [38]. According to SEM observations and due to the higher diffusivity of hydrogen at higher temperatures, this phenomenon occurs more frequently when the hydrogenation temperature is increased to 400 °C. As can be seen in Fig. 6, this phenomenon might be attributed to the presence of a spherical Nd-rich phase (which will be explained in section 3.2.1), which has sufficient strength to make a microindent impression on the matrix grain and might cause an additional force for crack initiation. In Fig. 6, a, b, and d, a clear microindent impression caused by the spherical Nd-rich phase can be seen, which could be an indication of the contribution of this phase to the initiation of intergranular cracks in the matrix grain during hydrogenation. As shown in Fig. 6, the indentation sites are in direct contact with the intergranular cracks, which increases the possibility of this hypothesis. This observation confirms that even low-temperature hydrogenation has the potential to cause sufficient deformation to induce intergranular cracks in the matrix grain of $Nd_2Fe_{14}B$, leading to a reduction in grain size. However, there is a difference between the intergranular cracks that form at lower and higher hydrogenation temperatures. At lower hydrogenation temperatures (e.g., Fig. 6, a), the energy of the cracks is insufficient to propagate to the edge of the grain, whereas, at higher hydrogenation temperatures (e.g., Fig. 6, c), the cracks easily cut through the grains from edge to edge. A reasonable explanation for this phenomenon could be that the diffusivity of hydrogen increases with temperature. In other words, at lower temperatures, hydrogen atoms have sufficient diffusivity to enter the interstitial sites in the $Nd_2Fe_{14}B$ unit cell but not enough to leave these sites, whereas at higher temperatures they can leave these trap sites and consequently have sufficient diffusivity to cut the grains.

Table 3 shows the average chemical composition of the $Nd_2Fe_{14}B$ matrix grain before and after low-temperature hydrogenation obtained by EDS point analysis. These data confirm that the matrix grain is far more resistant to oxidation than the Nd-rich phases. The lower amount of oxygen after hydrogenation at 400 °C compared to raw magnets can be because of longer exposure of raw magnets to the open air.

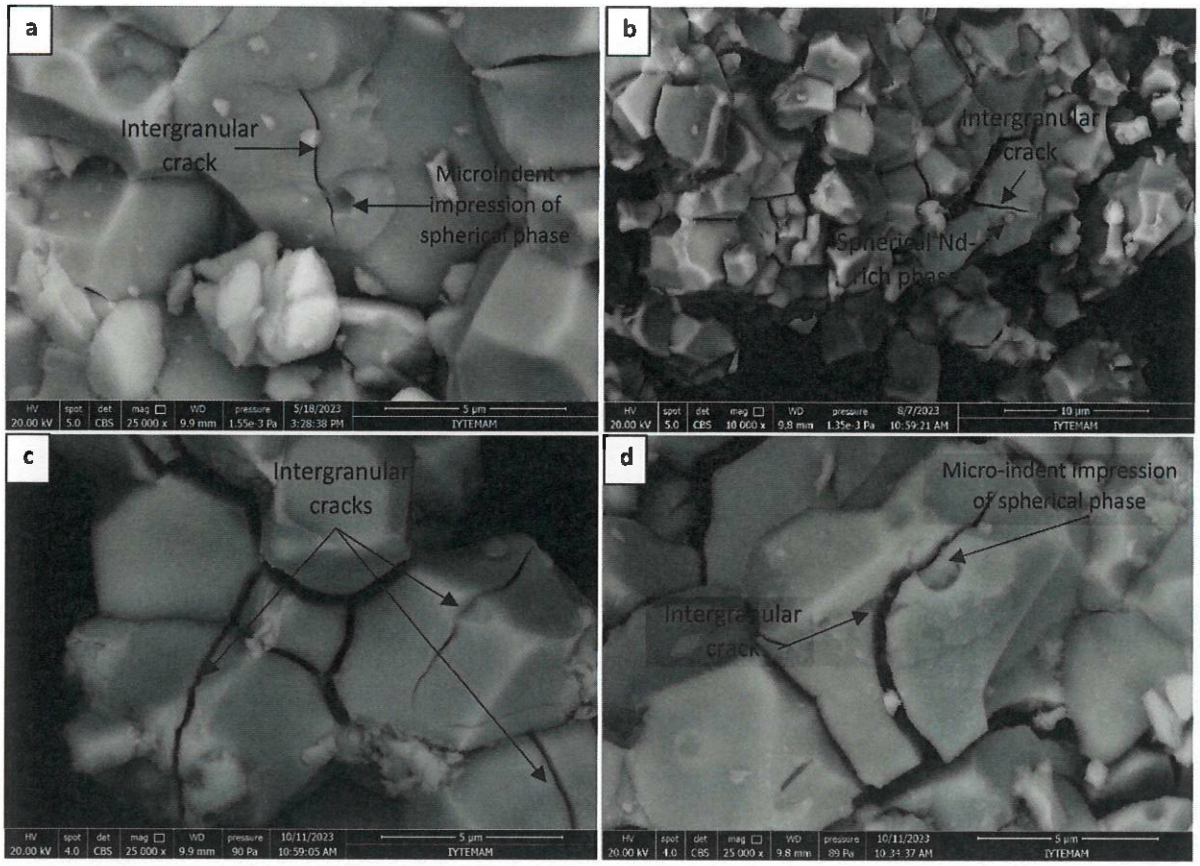



**Fig. 6)** BSE SEM images of intergranular cracks, spherical Nd-rich phase, and micro-indent impression of spherical phase in the matrix grain of $Nd_2Fe_{14}B$ after hydrogenation at **a)** 50 °C, **b)** 100 °C, **c)** 250 °C, and **d)** 400 °C

**Table 3)** Average chemical composition of $Nd_2Fe_{14}B$ matrix grain before and after low-temperature hydrogenation of NdFeB magnets, obtained by EDS point analysis

| Elements | Raw magnet | HD at 100 °C | HD at 200 °C | HD at 300 °C | HD at 400 °C |
|---|---|---|---|---|---|
| B | 0.00 | 1.04 | 2.39 | 0.06 | 0.00 |
| O | 6.00 | 2.22 | 2.14 | 1.12 | 3.90 |
| Fe | 62.75 | 66.65 | 67.85 | 68.73 | 67.18 |
| Pr | 5.46 | 5.05 | 4.48 | 4.91 | 4.81 |
| Nd | 25.79 | 25.04 | 23.13 | 25.18 | 24.12 |
| Dy | 0.00 | 0.00 | 0.00 | 0.00 | 0.00 |

## 3.2. Nd-rich phase

The cross-sectional SEM image of the broken magnet before hydrogenation (Fig. 2) confirms the presence of two distinct Nd-rich phases based on the morphology and distribution, including a spherical phase at the surface of the matrix grains and an Nd-rich grain boundary network comprising a semi-spherical Nd-rich phase in the triple junctions and a thin layer between the grains (labeled in Fig. 2). While the latter form a network of a grain boundary phase and are interconnected, the former is completely different in every respect.

### 3.2.1. Spherical Nd-rich Phase

**Before Hydrogenation:**

The small spherical particles on the surface of the matrix grains can be seen throughout the cross-section of the magnet before hydrogenation (labeled in Fig. 2). According to the EDS point analysis, the spherical Nd-rich phase

contains about 75 % Nd + Pr, the rest is iron, which absorbs about 1-2 % oxygen and can leave a distinct micro-indent impression (labeled in Fig. 2) on the matrix grain. Due to its spherical shape, it could originate from the liquid phase and not be remelted and evenly distributed in the microstructure. Since the initial chemical composition of Nd and Pr (27.2 wt%) is sufficient to form a continuous, interconnected grain boundary surrounding and isolating all matrix grains, the presence of a spherical phase can be attributed to an inefficient heat treatment process. In addition, the absence of alloying elements such as copper and aluminum can also lead to the formation of a spherical Nd-rich phase. Koyama et al [23] reported by increasing the copper content to 0.2 %, full coverage of matrix grain can be achieved by forming a eutectic composition.

**After Hydrogenation:**

Fig. 7 presents the spherical Nd-rich phase after hydrogenation at 100 and 400 °C, which proves the stability of this phase up to the maximum range of low-temperature hydrogenation. As shown in Fig. 7, the spherical Nd-rich phase with a size of about 1 µm did not undergo any change in terms of morphology and size during low-temperature hydrogenation up to 400 °C. The SEM image of this phase at higher magnification with secondary electrons (SE) (Fig. 7, a) shows a spherical Nd-rich phase at the edge of separation from the matrix grain due to the hydrogenation and pulverization of the magnet, indicating that there is no chemical bonding between this phase and the matrix grain. According to the SEM-EDS analysis at different temperatures, the spherical Nd-rich phase is the most stable compared to the others.

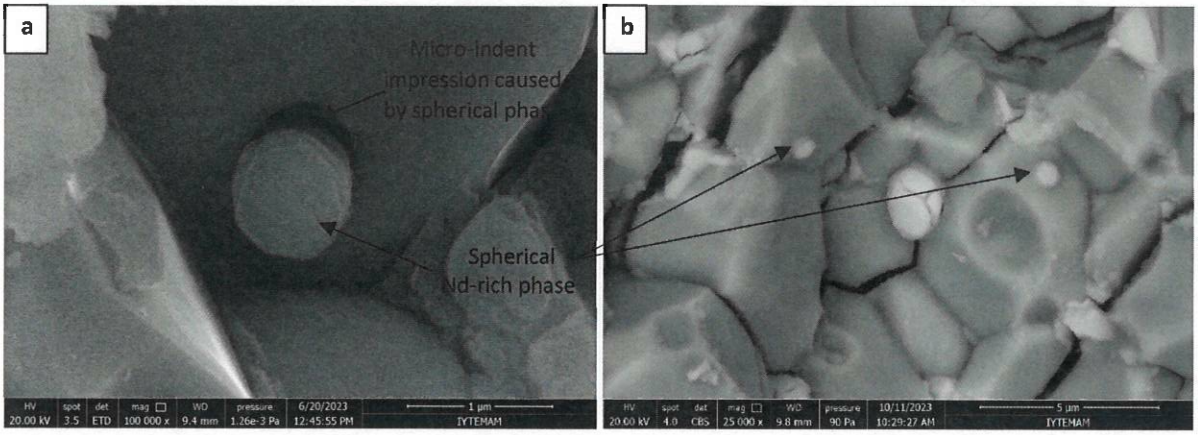



**Fig. 7)** SEM images of the spherical Nd-rich phase at the surface of matrix grains after low-temperature hydrogenation, **a)** at 100°C (SE SEM), and **b)** at 400°C (BSE SEM)

Table 4 represents the average chemical composition of the spherical Nd-rich phase after hydrogenation at different temperatures. The result shows that the oxygen content in this phase increases at lower hydrogenation temperatures and decreases at higher hydrogenation temperatures. This upward trend can be attributed to the increased formation of neodymium hydride at higher temperatures, which is a stable phase and reduces oxidation. In addition, the spherical Nd-rich phase absorbs less oxygen than other Nd-rich phases as the hydrogenation temperature increases. The other result of the EDS analysis is that Nd and Pr always occur together because they were extracted together from the earth. In addition, based on Table 2, the crystal structure of the spherical Nd-rich phase might be DHCP before and after hydrogenation at higher temperatures, while it is most probably FCC at lower temperatures [34].

**Table 4)** Average chemical composition of spherical Nd-rich phase before and after low-temperature hydrogenation of NdFeB magnets, obtained by EDS point analysis

| Elements | Raw magnet | HD at 25 °C | HD at 100 °C | HD at 200 °C | HD at 300 °C | HD at 400 °C |
|---|---|---|---|---|---|---|
| B | 0.00 | 0.00 | 1.06 | 0.00 | 0.33 | 0.00 |
| O | 4.83 | 17.31 | 18.64 | 19.75 | 4.68 | 10.22 |
| Fe | 34.90 | 29.31 | 16.70 | 19.06 | 31.52 | 26.01 |
| Pr | 10.04 | 8.42 | 11.78 | 7.70 | 11.97 | 11.41 |
| Nd | 50.23 | 44.96 | 51.82 | 52.87 | 51.49 | 52.36 |
| Dy | 0.00 | 0.00 | 0.00 | 0.62 | 0.00 | 0.00 |

### 3.2.2. Grain boundary Nd-rich Network

**Before Hydrogenation:**

The SEM cross-sectional image of the fractured magnet before hydrogenation (Fig. 2) shows a discontinued grain boundary network comprising an accumulated semi-spherical Nd-rich phase at the triple junctions and an uneven distribution of a thin Nd-rich layer between the matrix grains. Fig. 8, another cross-sectional SEM image of a just-broken NdFeB magnet before hydrogenation, shows that the morphology of the thin Nd-rich layer started to change when it was exposed to air before the SEM images were taken. Due to the high reactivity of Nd and Pr, this transition is most likely an oxidation. The semi-spherical Nd-rich phase (labeled in Fig. 8), which is located at the triple junctions and has an average size of 4 μm, contains about 80 % Nd and Pr, 20 % Fe, and can absorb about 10 % oxygen before hydrogenation.

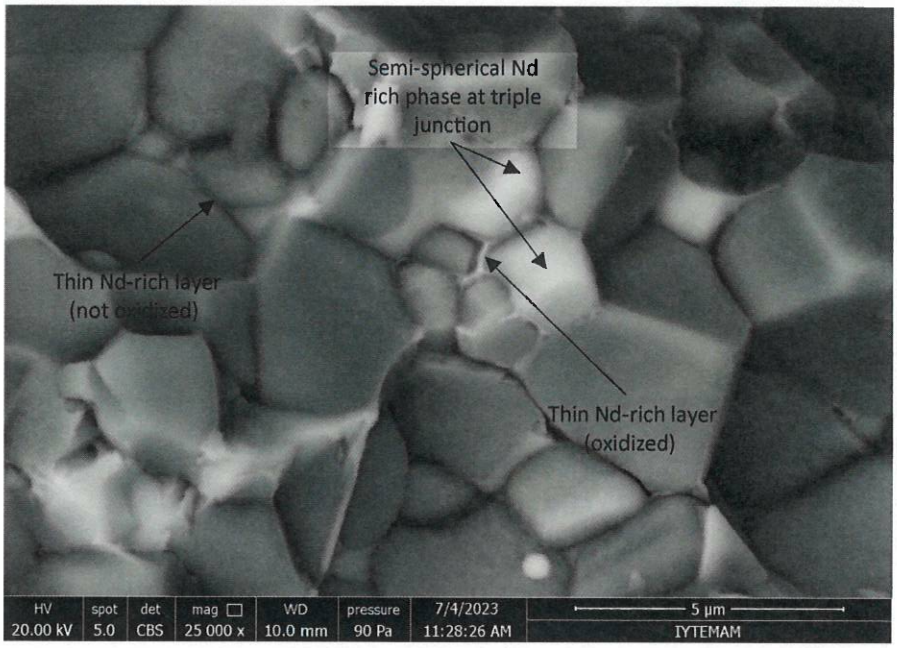



**Fig. 8)** Cross-sectional Backscattered Electron SEM (BSE SEM) image of the broken raw NdFeB magnet representing the Nd-rich grain boundary network.

**After Hydrogenation:**

Fig. 9 shows the microstructure of NdFeB magnets after hydrogenation at 100 °C at various magnifications. In this image, there is no trace of a thin Nd-rich layer left, and all the Nd in the thin grain boundary phase was either consumed to form neodymium hydride ($NdH_2$), which is consistent with the mechanism of hydrogenation or the formation of neodymium oxide ($Nd_2O3$) due to the high reactivity of neodymium, based on the X-ray diffractions shown in Fig. 4. Based on the results of EDS characterization and element mapping (Fig. 10), there is an Nd-rich phase that appears in a fuzzy form after hydrogenation, which is marked in Fig. 9 and Fig. 10 and will be referred to as the *Nd-rich cloudy phase* from now on. This phase has no regular shape and its only constant feature is the lack of rigidity. Fig. 11 shows that the Nd-rich cloudy phase is found everywhere like debris and even often in triple junctions which means that the semi-spherical phase can also be oxidized and transformed into the cloudy phase, even by hydrogenation at 50 °C. While the size of the Nd-rich cloudy phase in Fig. 11 a is less than 2 μm, it is about 4 μm in Fig. 11 b, and in general, it can be detected in a wide size range, with most cases being detected as clusters as marked with a yellow circle in Fig. 10.

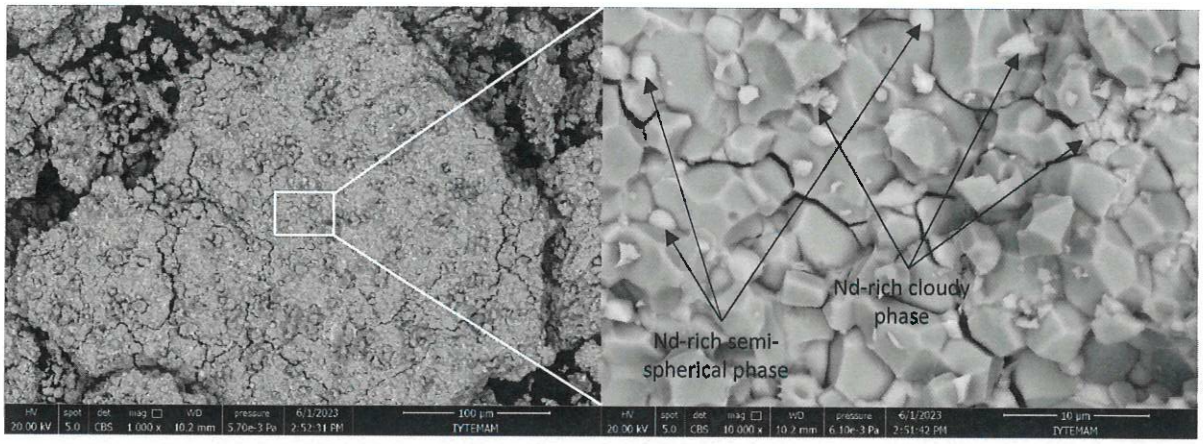



**Fig. 9)** BSE SEM images of the hydrogenated magnet at 100°C representing the Nd-rich cloudy phase

The elemental mapping presented in Fig. 10 confirms that the Nd-rich cloudy phase has a high oxygen content and therefore contains a considerable amount of neodymium oxide. This statement is supported by the EDS point analysis shown in Table 5, which confirms that the oxygen uptake of the Nd-rich cloudy phase after hydrogenation can reach 24% at lower temperatures and decrease to about 18 wt% at higher temperatures (above 350 °C). The lower oxidation at higher temperatures could be related to the formation of neodymium hydride. Without considering the oxygen content, the EDS results show that the Nd-rich cloudy phase contains 60-80 wt% Nd and Pr, while the rest is up to 100 wt% iron. Based on the reports by different researchers [20, 31, 34] the crystal structure of the Nd-rich cloudy phase might be FCC and contains neodymium oxide in the form of $Nd_2O_3$.

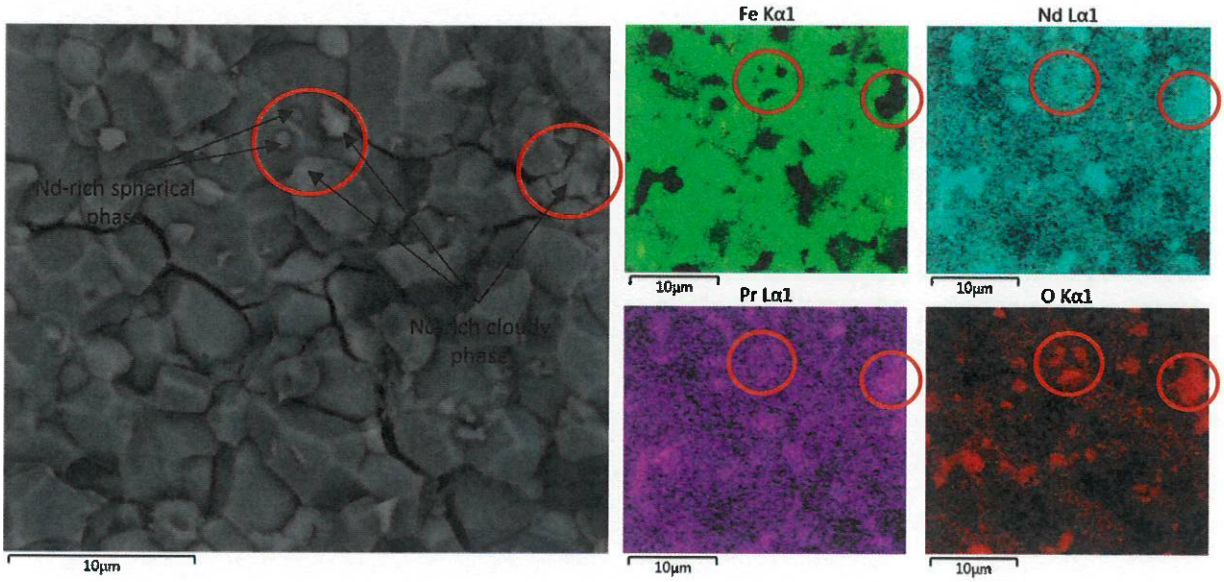



**Fig. 10)** BSE SEM images and elemental mapping of a hydrogenated magnet at 100°C.

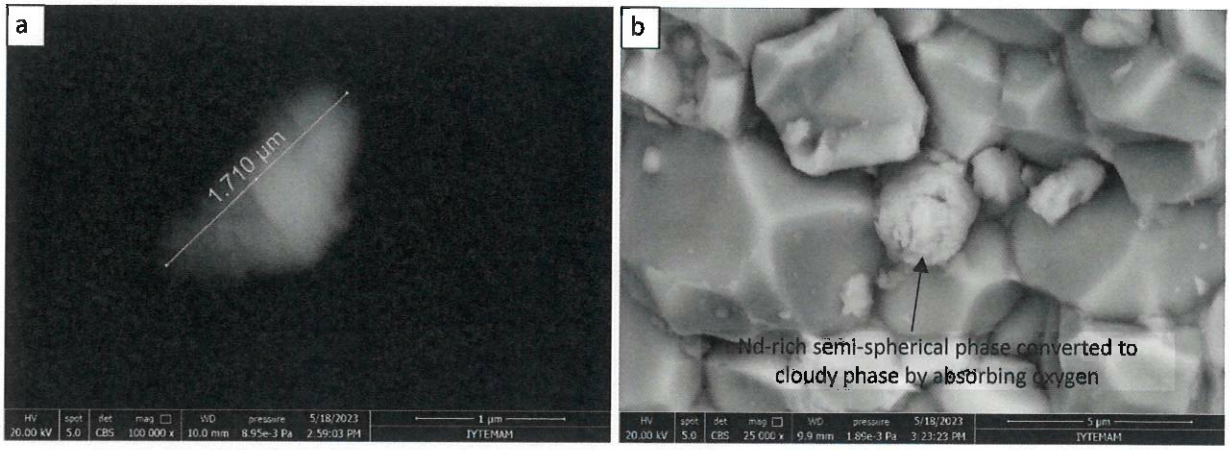



**Fig. 11)** BSE SEM images of the Nd-rich cloudy phase of the hydrogenated magnet at 50˚C in two different conditions, **a)** a flying debris of Nd-rich cloudy phase, and **b)** a former semi-spherical Nd-rich phase converted to cloudy phase at triple junction.

**Table 5)** Average chemical composition of Nd-rich cloudy phase after low-temperature hydrogenation obtained by EDS analysis

| Elements | HD at 25 ˚C | HD at 100 ˚C | HD at 200 ˚C | HD at 300 ˚C | HD at 400 ˚C |
|---|---|---|---|---|---|
| B | 0 | 0.15 | 0 | 0 | 0 |
| O | 16.62 | 24.42 | 23.34 | 24.09 | 18.7 |
| Fe | 13.9 | 15.11 | 11.79 | 19.79 | 18.2 |
| Pr | 17.3 | 12.38 | 13.82 | 10.36 | 12.19 |
| Nd | 52.18 | 47.94 | 50.68 | 45.77 | 50.91 |
| Dy | 0 | 0 | 0.37 | 0 | 0 |

The other part of the Nd-rich grain boundary network that accumulates at the triple junctions, which can be seen and recognized in Figs. 2, 8, and 9, was termed the *semi-spherical Nd-rich phase*. This phase underwent two opposite pathways during hydrogenation at different temperatures. In the first pathway, which is more common at lower temperatures, the semi-spherical Nd-rich particles absorb oxygen, and the oxygen content increases with increasing hydrogenation temperature (up to 200 ˚C) and even reaches 27 wt% and often turns into the cloudy phase. In the second path which usually takes place at a hydrogenation temperature above 200 ˚C, the semi-spherical Nd-rich phase absorbs less oxygen, which is a sign of hydrogen absorption and the formation of neodymium hydride.Consequently, the morphology of the phase changes into a *cupcake* structure due to the induced expansion by the formation of NdH2, as shown in Fig. 12. This morphology was not observed at temperatures below 200 ˚C, which contradicts the thermodynamics of neodymium hydride formation, as $NdH_2$ is more stable at room temperature [9].

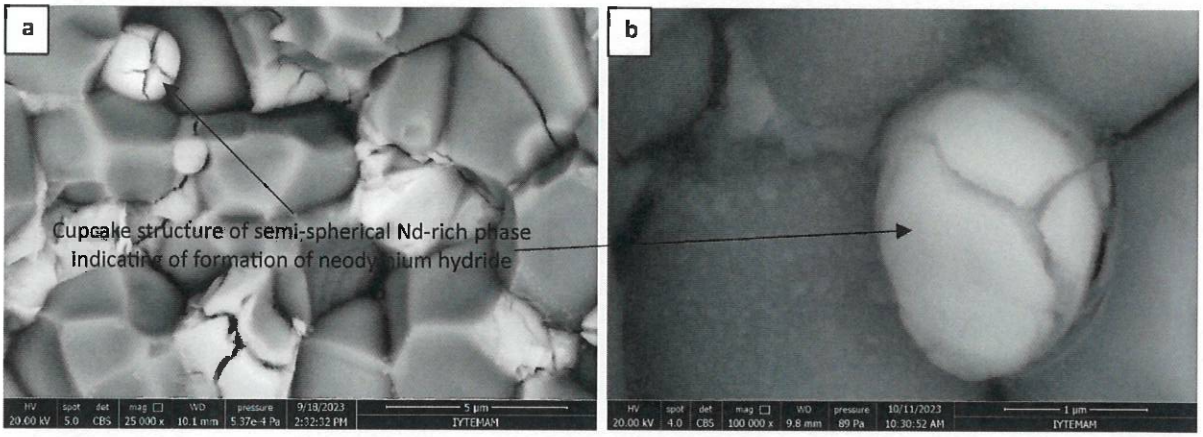



**Fig. 12)** BSE SEM images of the semi-spherical Nd-rich phase with a cupcake morphology indicating the formation of $NdH_2$ after hydrogenation at **a)** 350˚C, and **b)** 400 ˚C.

Table 6 presents the EDS point analysis of the average chemical composition of the semi-spherical Nd-rich phase at different hydrogenation temperatures. While the EDS results for a hydrogenation temperature of 400 °C were all from a semi-spherical Nd-rich phase with a cupcake structure, the result for a hydrogenation temperature of 200 °C was a mixture of normal and cupcake structures. The lower amount of oxygen after hydrogenation at 400 °C compared to the raw magnets may be due to the fact that the raw magnets were exposed to air for a longer time. Therefore, based on the report by Mo et al [20], the crystal structure of the semi-spherical Nd-rich phase with cupcake structure may be DHCP, while the normal structure with oxygen content above 9% is FCC structure and contains the neodymium oxide in the form of $Nd_2O_3$.

**Table 6)** Average chemical composition of semi-spherical Nd-rich phase before and after low-temperature hydrogenation of NdFeB magnets, obtained by EDS point analysis

| Elements | Raw magnet | HD at 25 °C | HD at 100 °C | HD at 200 °C | HD at 400 °C |
|---|---|---|---|---|---|
| B | 0.00 | 0.00 | 0.00 | 0.02 | 0.00 |
| O | 9.45 | 15.39 | 17.30 | 10.20 | 8.76 |
| Fe | 14.50 | 10.17 | 17.70 | 16.12 | 12.46 |
| Pr | 14.55 | 14.13 | 11.64 | 13.77 | 14.34 |
| Nd | 61.50 | 59.89 | 53.26 | 59.77 | 64.40 |
| Dy | 0.00 | 0.00 | 0.10 | 0.12 | 0.03 |

## Conclusion

The microstructural investigation of all phases and particles in the NdFeB magnets was performed before and after low-temperature hydrogenation in the range of 25 to 400 °C. The NdFeB magnets consist of two main phases, including the matrix grain of $Nd_2Fe_{14}B$ and the Nd-rich phase. The Nd-rich phase can occur in different morphologies and chemical compositions, including spherical particles, referred to as the spherical Nd-rich phase, and the grain boundary network, which in turn consists of a thin Nd-rich layer between the matrix grains and accumulated Nd at the triple junctions, referred to as semi-spherical Nd-rich phase. The $Nd_2Fe_{14}B$ matrix grain forms four different hydrides ($Nd_2Fe_{14}BH_x$) with different hydrogen content after low-temperature hydrogenation. When the hydrogenation temperature is increased up to 400 °C, the hydrogen index decreases due to the higher diffusivity of the hydrogen atoms, allowing them to escape the interstitial trap sites. At the same time, the finest particle size is reached when the hydrogen index is at its maximum. The spherical Nd-rich phase located on the surface of the matrix grains does not form a chemical bond with the matrix grain has sufficient strength and rigidity to leave a micro-indent impression on the surface of the matrix grain, and does not undergo any visible changes during the hydrogenation process up to 400 °C. Most of the Nd-rich phase was consumed to form a network of a thin grain boundary phase isolating the matrix grain; however, Nd accumulation occurred at the triple junctions prior to hydrogenation. During hydrogenation, most of the Nd-rich thin grain boundary phase absorbs oxygen and transforms into an Nd-rich cloudy phase. The semi-spherical Nd-rich phase forms mainly neodymium oxide at a hydrogenation temperature below 200 °C and hydride at a hydrogenation temperature above 200 °C. The formation of hydride is accompanied by the formation of a cupcake structure and local expansion. The oxygen uptake of all Nd-rich phases initially increases with increasing hydrogenation temperature up to 300 °C and then decreases, because of the formation of neodymium hydride, which is a stable phase against oxidation.

## Funding

This research was funded by the Scientific and Technological Research Council of Turkey (TÜBITAK) under the BIDEB-2232 program with grant number 118C311. In addition, the Environmental Research Center at İzmir Institute of Technology is gratefully acknowledged for metal analyses.

## Acknowledgments

The authors gratefully acknowledged the support from Exitcom Recycling Company for providing all needed samples.

## Declaration

**Conflict of Interest:** The authors declare that they have no conflict of interest.

## References

1. Sagawa, M., et al., *Permanent magnet materials based on the rare earth-iron-boron tetragonal compounds.* IEEE transactions on Magnetics, 1984. **20**(5): p. 1584-1589.
2. Zhou, B., Z. Li, and C. Chen, *Global potential of rare earth resources and rare earth demand from clean technologies.* Minerals, 2017. 7(11): p. 203.
3. Buschow, K., *Magnetism and processing of permanent magnet materials.* Handbook of magnetic materials, 1997. **10**: p. 463-593.
4. Binnemans, K., et al., *Recycling of rare earths: a critical review.* Journal of cleaner production, 2013. **51**: p. 1-22.
5. Europeia, C., *Communication from the Commission to the European Parliament, the Council, the European Economic and Social Committee and the Committee of the Regions Critical Raw Materials Resilience: Charting a Path towards Greater Security and Sustainability.* European Commission: Brussels, Belgium, 2020.
6. Dushyantha, N., et al., *The story of rare earth elements (REEs): Occurrences, global distribution, genesis, geology, mineralogy and global production.* Ore Geology Reviews, 2020. **122**: p. 103521.
7. Yang, Y., et al., *REE recovery from end-of-life NdFeB permanent magnet scrap: a critical review.* Journal of Sustainable Metallurgy, 2017. **3**: p. 122-149.
8. Karal, E., et al., *Hydrometallurgical recovery of neodymium from spent hard disk magnets: A life cycle perspective.* Journal of cleaner production, 2021. **288**: p. 125087.
9. Habibzadeh, A., M.A. Kucuker, and M. Gökelma, *Review on the Parameters of Recycling NdFeB Magnets via a Hydrogenation Process.* ACS Omega, 2023.
10. Walton, A., et al., *The use of hydrogen to separate and recycle neodymium–iron–boron-type magnets from electronic waste.* Journal of Cleaner Production, 2015. **104**: p. 236-241.
11. Piotrowicz, A., et al., *The use of thermal hydrogen decrepitation to recycle Nd-Fe-B magnets from electronic waste.* Journal of Mining and Metallurgy, Section B: Metallurgy, 2020. **56**(3): p. 415-424.
12. Michalski, B., et al., *Experimental evidence for the suitability of the hydrogen decomposition process for the recycling of Nd-Fe-B sintered magnets.* Journal of Magnetism and Magnetic Materials, 2022. **548**: p. 168979.
13. Isnard, O., et al., *Neutron-diffraction study of the insertion scheme of hydrogen in Nd2Fe14B.* Journal of applied physics, 1995. 78(3): p. 1892-1898.

14. Ram, S., et al., *Formation of Nd 2 Fe 14 B hydride by milling of anhydride particles in toluene in a closed reactor.* Bulletin of materials science, 1997. **20**: p. 1049-1058.

15. Önal, M.A.R., et al., *Comparative oxidation behavior of Nd-Fe-B magnets for potential recycling methods: Effect of hydrogenation pre-treatment and magnet composition.* Journal of Alloys and Compounds, 2017. **728**: p. 727-738.

16. Sepehri-Amin, H., S. Hirosawa, and K. Hono, *Advances in Nd-Fe-B based permanent magnets*, in *Handbook of magnetic materials*. 2018, Elsevier. p. 269-372.

17. Vial, F., et al., *Improvement of coercivity of sintered NdFeB permanent magnets by heat treatment.* Journal of magnetism and magnetic materials, 2002. **242**: p. 1329-1334.

18. Herbst, J.F., et al., *Relationships between crystal structure and magnetic properties in Nd 2 Fe 14 B.* Physical Review B, 1984. **29**(7): p. 4176.

19. Rong, C. and B. Shen, *Nanocrystalline and nanocomposite permanent magnets by melt spinning technique.* Chinese Physics B, 2018. **27**(11): p. 117502.

20. Mo, W., et al., *Dependence of the crystal structure of the Nd-rich phase on oxygen content in an Nd–Fe–B sintered magnet.* Scripta Materialia, 2008. **59**(2): p. 179-182.

21. Prokofev, P.A., et al., *Blending powder process for recycling sintered Nd-Fe-B magnets.* Materials, 2020. **13**(14): p. 3049.

22. Lucas, J., et al., *Rare earths: science, technology, production and use*. 2014: Elsevier.

23. Koyama, T., Y. Tsukada, and T. Abe, *Computational thermodynamics and microstructure simulations to understand the role of grain boundary phase in Nd-Fe-B hard magnets.* Science and Technology of Advanced Materials, 2021. **22**(1): p. 1-13.

24. Nishizawa, T., *Thermodynamics of microstructures*. 2008: Asm International.

25. Sepehri-Amin, H., et al., *Grain boundary and interface chemistry of an Nd–Fe–B-based sintered magnet.* Acta Materialia, 2012. **60**(3): p. 819-830.

26. Lv, M., et al., *Progress on modification of microstructures and magnetic properties of Nd-Fe-B magnets by the grain boundary diffusion engineering.* Journal of Magnetism and Magnetic Materials, 2021. **517**: p. 167278.

27. Zhou, T., et al., *Sintered NdFeB magnets with Tb-Dy double-layer core/shell structure were fabricated by double alloy method and grain boundary diffusion.* Journal of Alloys and Compounds, 2021. **856**: p. 158191.

28. Tang, W., et al., *An investigation of the Nd-rich phases in the Nd-Fe-B system.* Journal of applied physics, 1988. **64**(10): p. 5516-5518.

29. Wang, G., et al., *Mechanical properties and the composition of Nd-rich phase in sintered Nd-Fe-B magnets prepared by spark plasma sintering.* Journal of Magnetism and Magnetic Materials, 2019. **486**: p. 165261.

30. Xin, F., et al., *Microstructural investigation of Nd-rich phase in sintered Nd-Fe-B magnets through electron microscopy.* Journal of Rare Earths, 2013. **31**(8): p. 765-771.

31. Li, W., T. Ohkubo, and K. Hono, *Effect of post-sinter annealing on the coercivity and microstructure of Nd–Fe–B permanent magnets.* Acta Materialia, 2009. **57**(5): p. 1337-1346.

32. Sasaki, T., T. Ohkubo, and K. Hono, *Structure and chemical compositions of the grain boundary phase in Nd-Fe-B sintered magnets.* Acta Materialia, 2016. **115**: p. 269-277.

33. Shinba, Y., et al., *Transmission electron microscopy study on Nd-rich phase and grain boundary structure of Nd–Fe–B sintered magnets.* Journal of applied physics, 2005. **97**(5).

34. Yin, X., I. Jones, and I. Harris, *The microstructural characterisation of Nd-Fe-B alloys. II: Microstructural investigation of cast Nd-Fe-B materials.* Journal of magnetism and magnetic materials, 1993. **125**(1-2): p. 91-102.

35. Wang, S. and Y. Li, *In situ TEM study of Nd-rich phase in NdFeB magnet.* Journal of Magnetism and Magnetic Materials, 2005. **285**(1-2): p. 177-182.

36. Li, X., et al., *Effect of hydrogen pressure on hydrogen absorption of waste Nd-Fe-B sintered magnets.* Journal of Magnetism and Magnetic Materials, 2019. **473**: p. 144-147.

37. Li, C., et al., *Recycling of scrap sintered Nd–Fe–B magnets as anisotropic bonded magnets via hydrogen decrepitation process.* Journal of Material Cycles and Waste Management, 2015. **17**(3): p. 547-552.

38. Kilner, J.A., et al., *Functional materials for sustainable energy applications.* 2012: Elsevier.